

ORIGINAL ARTICLE

Open Access



A Hyper-redundant Elephant's Trunk Robot with an Open Structure: Design, Kinematics, Control and Prototype

Yongjie Zhao^{1*} , Xiaogang Song¹, Xingwei Zhang¹ and Xinjian Lu²

Abstract

As for the complex operational tasks in the unstructured environment with narrow workspace and numerous obstacles, the traditional robots cannot accomplish these mentioned complex operational tasks and meet the dexterity demands. The hyper-redundant bionic robots can complete complex tasks in the unstructured environments by simulating the motion characteristics of the elephant's trunk and octopus tentacles. Compared with traditional robots, the hyper-redundant bionic robots can accomplish complex tasks because of their flexible structure. A hyper-redundant elephant's trunk robot (HRETR) with an open structure is developed in this paper. The content includes mechanical structure design, kinematic analysis, virtual prototype simulation, control system design, and prototype building. This design is inspired by the flexible motion of an elephant's trunk, which is expansible and is composed of six unit modules, namely, 3UPS-PS parallel in series. First, the mechanical design of the HRETR is completed according to the motion characteristics of an elephant's trunk and based on the principle of mechanical bionic design. After that, the backbone mode method is used to establish the kinematic model of the robot. The simulation software SolidWorks and ADAMS are combined to analyze the kinematic characteristics when the trajectory of the end moving platform of the robot is assigned. With the help of ANSYS, the static stiffness of each component and the whole robot is analyzed. On this basis, the materials of the weak parts of the mechanical structure and the hardware are selected reasonably. Next, the extensible structures of software and hardware control system are constructed according to the modular and hierarchical design criteria. Finally, the prototype is built and its performance is tested. The proposed research provides a method for the design and development for the hyper-redundant bionic robot.

Keywords: Hyper-redundant elephant's trunk robot, Mechanical structure design, Kinematic analysis, Virtual prototype simulation, Control system, Prototype building

1 Introduction

With the introduction of the concept of Industry 4.0, robots have become more and more essential in intelligent manufacturing [1]. Despite the wide application of robots in the industry [2–5], medical sector [6–10], aerospace field [11, 12], and other fields, consumers' needs are becoming increasingly dynamic and complex [13]. This challenge can be resolved with better motion

flexibility, stiffness and load capacity of robots. While traditional robots cannot meet the flexible demands of users, bionic robots can simulate the motion characteristics of elephant's trunk and octopus tentacles efficiently. Compared with traditional robots, the hyper-redundant bionic robots can accomplish complex tasks in unstructured environments with narrow workspace and numerous obstacles because of their flexible structure [14]. These contemporary robots have attracted the attention of industry experts and researchers [15–19].

Having the capability to complete complex tasks in unstructured environments by simulating the motion characteristics of the elephant's trunk and octopus

*Correspondence: meijzhao@stu.edu.cn

¹ Department of Mechatronics Engineering, Shantou University, Shantou 515063, China

Full list of author information is available at the end of the article

tentacles, bionic robots can be divided into two categories: (1) Continuous robots are a kind of machines that are driven by flexible and extensible materials such as elastic links and biological muscles [20]. Jones et al. [21] developed a continuous robot driven by both pneumatic and tendon by observing the motion principle of tentacles and elephant's trunks. The flexible motion control of the robot was achieved based on the new kinematic modeling method. In order to improve the flexibility and adaptability of the robot in an unknown environment, Wang et al. [22] proposed a cable-driven continuous robot. They established its kinematic model and controlled it by a visual servo system. Eventually, Lyapunov theory was used to prove the stability of the control system. Continuous robots can bend continuously like invertebrates and avoid obstacles flexibly. However, the structure construction and the precise position control of such robots are difficult to achieve practically. What's more, the load capacity of continuous robots is relatively low because of structural limitations. (2) The hyper-redundant robots are a type of robots, which are in series with single-degree-of-freedom driving joints or in series with 2-4-degree-of-freedom parallel mechanism unit modules [23]. Transteth et al. [24, 25] studied the obstacle-crossing gait of snakes and developed a snake-like robot Aiko with high flexibility and adaptability. This robot can survey many unknown and complex terrains and can carry out rescue missions in the rubble. Gallardo et al. [26] developed an open-structured hyper-redundant robot with a 3-DOF parallel mechanism as a unit module. Screw theory was employed to analyze the kinematics of this robot. Finally, a 30-DOF robot was used as an example to show that this robot has good motion performance. Taherifaret [27] proposed a hyper-redundant elephant's trunk robot driven by a hydraulic system. The robot realizes the motion of the end moving platform through the control of the hydraulic valve, which has the advantages of high stiffness and strong load capacity. Generally, the flexibility of hyper-redundant robots is not as efficient as that of continuous robots. However, because of rigid rods and motors, hyper-redundant robots have better stiffness and load capacity, and they are easier to achieve accurate position control when accomplishing complex operational tasks in the unstructured environment with narrow workspace and numerous obstacles. Especially in the ocean environment, the buoyancy of seawater counteracts gravity effect of the robot to a certain extent, the dynamic performance of these kinds of robots can be better, so the hyper-redundant robots have broad application prospects in the ocean monitoring, deep-sea exploration and other fields. The motivation of the paper is to present the development of the HRETR with an open structure including mechanical structure design,

kinematic analysis, virtual prototype simulation, control system design, and prototype building.

In this paper, a HRETR with an open structure, which is composed of six 3UPS-PS parallel mechanism unit modules in series, is built based on the principle of mechanical bionics and based on the special structure characteristics and motion mechanism of an elephant's trunk muscle group. The main content in this paper includes the overall conception, mechanism design, kinematic model, virtual prototype, control system, physical prototype construction, and performance testing. The rest of this paper is arranged as follows. In Section 2, the mechanical structure design and the overall configuration layout are introduced. In Section 3, the kinematic modeling method of the robot is elaborated. In Section 4, virtual prototype technology is used to carry out the dynamic and static stiffness analysis of the robot. In Section 5, the design of software and hardware of the control system is presented. In Section 6, the construction and performance test of the prototype are introduced, and the performance of the prototype is summarized. Finally, the conclusion is drawn in Section 7.

2 Mechanical Structure Design

The hyper-redundant elephant's trunk robot is based on the analysis of the external shape and the motion mechanism of an elephant's trunk. The hyper-redundant robot is applied to imitate the motion characteristics of an elephant's trunk. Therefore, the structural design of the HRETR mainly includes two sections: the overall configuration layout and the structural design of the unit module. Both determine the number of modules according to the connection mode of each unit module and functional requirements.

2.1 Mechanical Structure Design of the Unit Module

Elephants can grasp things flexibly with their trunk, which can achieve various irregular bending forms. A small segment of an elephant's trunk is taken as the research object. The cartilage and muscle tissues are distributed around the two expiratory holes. The trunk can move axially and bend radially by contracting the cartilage and muscle. The larger plane of the small segment will represent the reference plane. With the smaller one regarded as the moving plane and the center normal vector of the reference plane regarded as the z -axis, the coordinate system is established. The motion plane can move along the z -axis and rotate around three coordinate axes within a certain range. The motion schematic diagram is shown in Figure 1.

According to the physiological and motion characteristics of an elephant's trunk, a 3UPS-PS parallel mechanism (see Figure 2) is designed to complete the

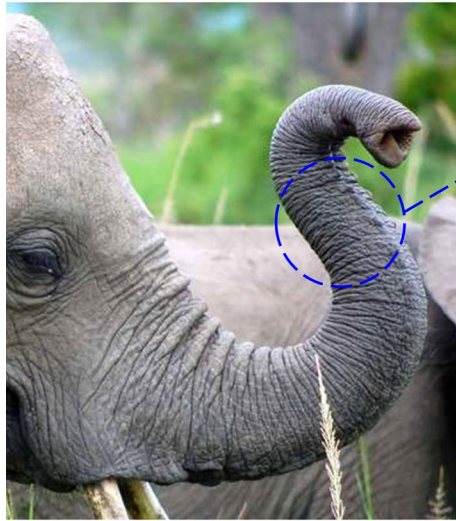


Figure 1 Posture of elephant's trunk

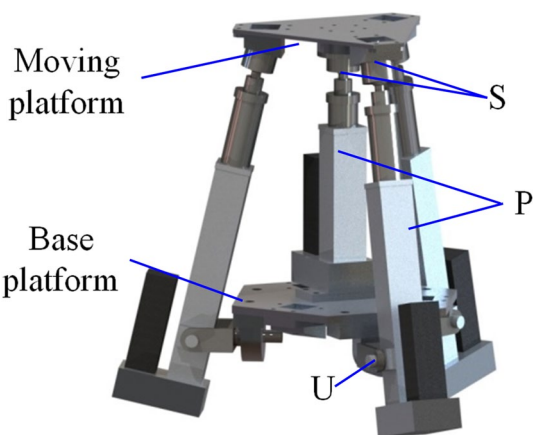
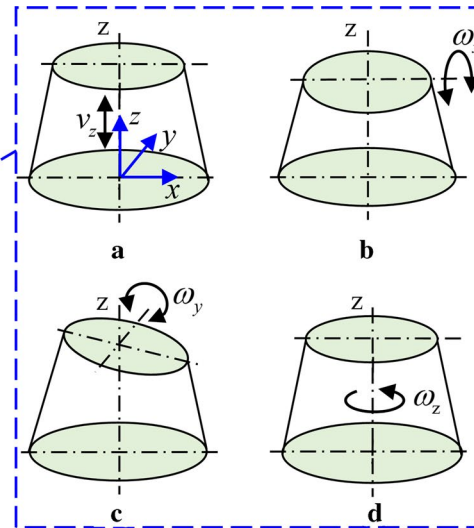


Figure 2 3UPS-PS unit module

three-dimensional rotation and one-dimensional movement of the small segment of an elephant's trunk. Taking 3UPS-PS parallel mechanism as a unit module has the advantages of high stiffness and high load-weight ratio [28–30]. The mechanism consists of a moving platform, a base platform, and four motion limbs. The central limb is PS limb and three external limbs are UPS limb. Here, the U, P, and S denote universal, prismatic, and spherical joints, respectively, and the underline denotes the driving joint. The moving platform of the parallel mechanism can perform three-dimensional rotation and one-dimensional movement within a certain range by changing the length of the four driving limbs, which corresponds to

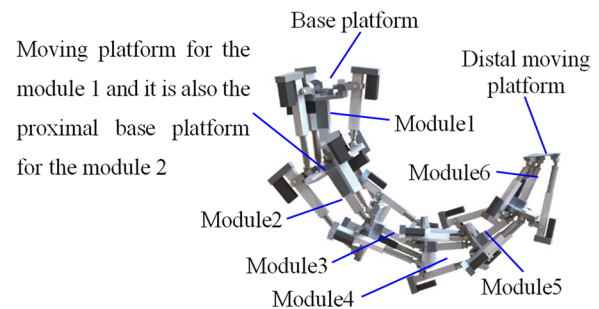


Figure 3 Integral configuration of HRETR

the four motion forms of an elephant's trunk. Drive mode adopts the servo-electric cylinder.

2.2 Integral Configuration Design of the HRETR

The overall configuration of the HRETR comprises several 3UPS-PS parallel mechanism modules in series based on the research and analysis of the structural characteristics, motion mechanism of an elephant's trunk, and the principle of miniaturization and lightweight. A 7-point coplanar design criterion (the rotating centers of spherical joints of the former unit module are coplanar with the rotating center of the universal joint of the latter unit module) is adopted for the convenience of kinematics and dynamics modeling. The connecting mode of the unit modules is in the form of staggered 60 degrees between the head and the tail to avoid mutual interference (Figure 3) in order to realize a 360-degree rotation of the moving platform of the HRETR. Besides, six

3UPS-PS parallel mechanism modules are connected in series according to engineering practice experience and considering the constraint of the rotation angle of the spherical joint ($\pm 35^\circ$). The size of the HRETR decreases accordingly.

3 Kinematic Analysis of the HRETR

3.1 Position Analysis of the HRETR

3.1.1 Spatial Backbone Curve

The basic idea of the backbone modal method is based on differential geometry theory [12]. The mode equation of the curve is constructed by mode sub-function and mode parameters.

The expression of the spatial curve is shown in Eq. (1). The integral form of the whole center line of the HRETR is described by the backbone modal method.

$$\mathbf{P}(s) = \int_0^s \mathbf{L}\boldsymbol{\kappa}(s) ds, \quad (1)$$

where $s \in [0, 1]$, L denotes the arc length of the curve, $\boldsymbol{\kappa}(s)$ represents the tangential vector of the spatial curve at s , $\alpha(s)$ denotes the angle between the y -axis and the projection of the vector $\boldsymbol{\kappa}(s)$ projecting on the $x_k O_k y_k$ plane, and $\beta(s)$ denotes the angle between the $\boldsymbol{\kappa}(s)$ and the $x_k O_k y_k$ plane. According to Figure 4, Eq. (1) can be expanded as:

$$\mathbf{p}(s) = \begin{bmatrix} \int_0^s L \sin \alpha(s) \cos \beta(s) ds \\ \int_0^s L \cos \alpha(s) \cos \beta(s) ds \\ \int_0^s L \sin \beta(s) ds \end{bmatrix} \quad (2)$$

Based on the mode function, $\alpha(s)$ and $\beta(s)$ can be parameterized as follows:

$$\begin{cases} \alpha(s) = \sum_{i=1}^{n_1} a_i f_i(s) + \sum_{i=1}^2 b_{i\alpha} g_i(s), \\ \beta(s) = \sum_{i=n_1+1}^{n_2} a_i f_i(s) + \sum_{i=1}^2 b_{i\beta} g_i(s), \end{cases} \quad (3)$$

where a_i denotes the mode synergetic parameter, n_1 refers to the number of the modal function related to $\alpha(s)$, n_2 represents the total number of the modal function, $b_{i\alpha}$ and $b_{i\beta}$ denote the auxiliary control parameters of the orientation angle, $f_i(s)$ is the modal sub-function, and $g_i(s)$ is the auxiliary orientation control function of the orientation angle of the backbone curve. Generally, functions $g_i(s)$ and $f_i(s)$ can usually be initialized as $f_1(s) = s$, $f_2(s) = 1$, $f_3(s) = s$, $f_4(s) = \sin(2\pi s)$,

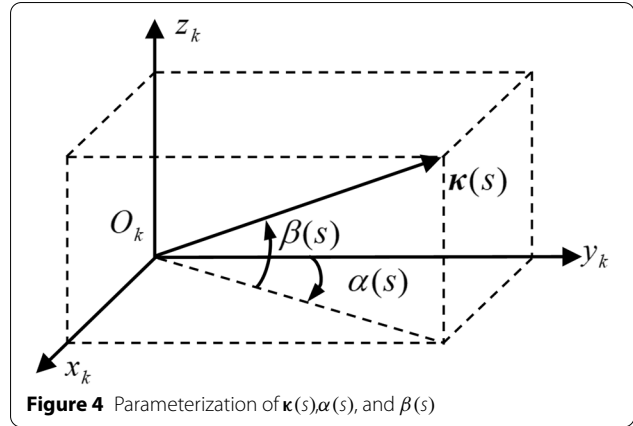


Figure 4 Parameterization of $\boldsymbol{\kappa}(s)$, $\alpha(s)$, and $\beta(s)$

$g_1(s) = 1 - \sin(\pi s/2)$, and $g_2(s) = \sin(\pi s/2)$. The configuration of the backbone is restricted by at least 3 linearly independent modal functions because the endpoint of the spatial curve is with three-dimensional geometric constraints. The initial modal function can be defined as:

$$\begin{cases} \alpha(s) = a_1 s + a_2 + b_{1\alpha} [1 - \sin(\pi s/2)] + b_{2\alpha} \sin(\pi s/2), \\ \beta(s) = a_3 s + a_4 \sin(2\pi s) + b_{1\beta} [1 - \sin(\pi s/2)] + b_{2\beta} \sin(\pi s/2). \end{cases} \quad (4)$$

After parameterization, $\mathbf{p}(s)$ is mainly related to a_i , $b_{i\alpha}$, and $b_{i\beta}$, and the configurations of the backbone curve can be obtained by the searching parameters a_i , $b_{2\alpha}$, and $b_{2\beta}$. The iteration approach can be used to search the appropriate control parameters, as given in Eq. (5):

$$\mathbf{c}_{m+1} = \mathbf{c}_m + \lambda \mathbf{J}_c^+(\mathbf{c}_m, 1)(\mathbf{v}_D - \mathbf{v}_m(1)), \quad (5)$$

where $\mathbf{c}_m = [a_{1m} \ a_{2m} \ a_{3m} \ a_{4m} \ b_{2\alpha m} \ b_{2\beta m}]^T$ denotes the position and orientation control parameters of the spatial backbone curve at s , a_{1m} , a_{2m} , a_{3m} , a_{4m} , $b_{2\alpha m}$, and $b_{2\beta m}$ denote the value of a_1 , a_2 , a_3 , a_4 , $b_{2\alpha}$, and $b_{2\beta}$ iterating m times respectively, λ is a positive constant that controls the convergence of the iterative equation, $\mathbf{v}_m(s) = [\mathbf{p}(s)^T \ \alpha(s) \ \beta(s)]^T$ refers to the vector of the position and orientation angle at s , \mathbf{v}_D is the target configuration. \mathbf{J}_c is not a square matrix, \mathbf{J}_c^+ is a pseudo-inverse matrix of \mathbf{J}_c .

$$\mathbf{J}_c(\mathbf{c}, s) = \frac{\partial \mathbf{v}_m(s)}{\partial \mathbf{c}_m} = \begin{bmatrix} \frac{\partial v_{m1}}{\partial c_{m1}} & \frac{\partial v_{m1}}{\partial c_{m2}} & \dots & \frac{\partial v_{m1}}{\partial c_{m6}} \\ \frac{\partial v_{m2}}{\partial c_{m1}} & \frac{\partial v_{m2}}{\partial c_{m2}} & & \\ \vdots & & \ddots & \\ \frac{\partial v_{m5}}{\partial c_{m1}} & & & \frac{\partial v_{m5}}{\partial c_{m6}} \end{bmatrix}_{5 \times 6}. \quad (6)$$

3.1.2 Spatial Backbone Fitting

The spatial backbone curve equation is constructed based on the searched parameters. Searched by dichotomy are

the fitting points of the center of the moving platform on the backbone curve of each parallel mechanism module of the HRETR. The variable \mathbf{p}_k denotes the vector from the center of the moving platform of k th parallel mechanism module to the $(k-1)$ th parallel mechanism module. Because the base parallel mechanism module is mounted vertically on the fixed frame, the fitting point of the moving platform position cannot be on the spatial backbone curve, $\mathbf{p}_1 = [0 \ 0 \ -l_1]^T$. The length of the i th limb of the k th parallel module need to meet the following requirement:

$$l_{b,ki} \leq q_{ki} \leq l_{r,ki} + l_{b,ki}, \quad (i = 0, 1, 2, 3; \quad k = 1, 2, \dots, n), \quad (7)$$

where $l_{b,ki}$ and $l_{r,ki}$ denote the length of the sleeve and the push rod of the i th limb, respectively. Also, L_c represents the length of the middle limb which can be writing as follows:

$$L_c = \begin{bmatrix} l_{r,10} & 0 & 0 \\ 0 & l_{r,20} & 0 \\ & & \ddots & \vdots \\ 0 & 0 & 0 & l_{r,n0} \end{bmatrix} \mathbf{H} + \begin{bmatrix} l_{b,10} \\ l_{b,20} \\ \vdots \\ l_{b,n0} \end{bmatrix}, \quad (8)$$

where $\mathbf{H} = [h_1 \ h_2 \ \dots \ h_n]^T$ is the parameters for controlling the length of the middle limbs. In each iteration, the parameter $h_i (i \in (1, n))$ is randomly selected between 0 and 1. When the lengths of other limbs obtained by the inverse displacement of the fitted parallel mechanism module do not satisfy the constraint conditions, the parameter \mathbf{H} can be adjusted to search again. The variable ${}^0\mathbf{R}_{O_k}$, which is defined by the Euler angle, denotes the rotation matrix of the moving platform of the k th parallel mechanism module.

$${}^0\mathbf{R}_{O_k} = \text{Rot}(y, \phi_{yk}) \text{Rot}(x, \phi_{xk}) \text{Rot}(z, \phi_{zk}). \quad (9)$$

Assuming $\mathbf{n}_k = [n_{k,x} \ n_{k,y} \ n_{k,z}]^T$ denotes the unit normal vector of the moving platform of the k th parallel mechanism module in the base coordinate system $O_0 - x_0y_0z_0$. As \mathbf{n}_k is equal to the third column of ${}^0\mathbf{R}_{O_k}$, it can be obtained as:

$$\begin{cases} \phi_{xk} = -\arctan(n_{k,y}/n_{k,z}), \\ \phi_{yk} = \arcsin(n_{k,x}), \\ \text{if } n_{k,z} < 0, \text{ let } \phi_{xk} = \phi_{xk} + \pi. \end{cases} \quad (10)$$

Equation (10) is not relevant to ϕ_{zk} , hence, the target orientation of each parallel module can be pre-set based on a suitable weight.

In sum, the transformation matrix ${}^{k-1}\mathbf{T}$ of the position and orientation of the moving platform, which is relative to the base platform in the k th parallel mechanism module, can be described as:

$${}^{k-1}\mathbf{T} = \begin{bmatrix} {}^{O_{k-1}}\mathbf{R}_{O_k} & \mathbf{p}_k \\ \mathbf{0}_{1 \times 3} & 1 \end{bmatrix}. \quad (11)$$

3.1.3 Inverse Kinematics of the Parallel Mechanism Module

The coordinate systems $O_{k-1} - x_{k-1}y_{k-1}z_{k-1}$ and $O_k - x_ky_kz_k$ are established at the geometric center of the base platform and the moving platform of the k th parallel mechanism module, respectively. The position vector equation of the i th limb of the k th parallel mechanism module is

$$q_{ki}\mathbf{e}_{k0} + {}^{O_{k-1}}\mathbf{R}_{O_k} \mathbf{b}_{ki} = \mathbf{a}_{ki} + q_{ki}\mathbf{e}_{ki}, \quad (12)$$

where $i = 1, 2, 3$, $k = 1, 2, 3, \dots, n$, \mathbf{a}_{ki} denotes the vector from the origin of the coordinate system $O_{k-1} - x_{k-1}y_{k-1}z_{k-1}$ to the center of the universal joint, \mathbf{b}_{ki} represents the vector from the origin of the coordinate system $O_k - x_ky_kz_k$ to the center of the spherical joint.

3.2 Velocity and Acceleration Analysis of the HRETR

The specific kinematic solution of the HRETR is as follows:

- 1) It involves providing the position and orientation x, y, z, ϕ_x, ϕ_y , and ϕ_z of the distal moving platform of the HRETR.
- 2) The inverse displacement algorithm of the HRETR based on the spatial backbone curve modal method is used to obtain the position and orientation of the moving platform relative to the base platform of each parallel mechanism module before interpolating the trajectory in the joint space.
- 3) It involves taking the time derivative of the trajectory, linear velocity \mathbf{v}_k , angular velocity $\boldsymbol{\omega}_k$, linear acceleration $\dot{\mathbf{v}}_k$, and angular acceleration $\dot{\boldsymbol{\omega}}_k$ of the moving platform of the k th unit module.
- 4) The kinematics of the HRETR is transformed into that of the unit module. The velocity and acceleration of each limb of the unit module are obtained by the inverse kinematics of the unit module.

$$\dot{\mathbf{q}}_{ki} = [\dot{q}_{k1} \ \dot{q}_{k2} \ \dot{q}_{k3} \ \dot{q}_{k4}]^T = \mathbf{J}_k \begin{bmatrix} \mathbf{v} \\ \boldsymbol{\omega} \end{bmatrix}, \quad (13)$$

$$\ddot{\mathbf{q}}_{ki} = \mathbf{J}_k \begin{bmatrix} \dot{\mathbf{v}} \\ \dot{\boldsymbol{\omega}} \end{bmatrix} + \mathbf{U}, \quad (14a)$$

$$U_{ki} = q_{ki}(\boldsymbol{\omega}_{ki}^T \boldsymbol{\omega}_{ki}) + (\mathbf{w}_{ki}^T \boldsymbol{\omega})(\boldsymbol{\omega}^T \mathbf{a}_{ki}) - (\mathbf{w}_{ki}^T \mathbf{a}_{ki})(\boldsymbol{\omega}^T \boldsymbol{\omega}), \quad (14b)$$

where J_k is the velocity of the Jacobian matrix, ω_{ki} and a_{ki} are the angular velocity of the limb in the basic coordinate system of the unit module and the coordinates of the hinge points of the moving platform, respectively.

The kinematic analysis method of the HRETR is designed according to the content shown in Figure 5.

4 Virtual Prototype Simulation

In the process of prototype development, the virtual prototype simulation technology of robots can be used in the whole life cycle of product development or system design, which includes feasibility demonstration, technical performance index determination, system design, equipment operation, and maintenance among others.

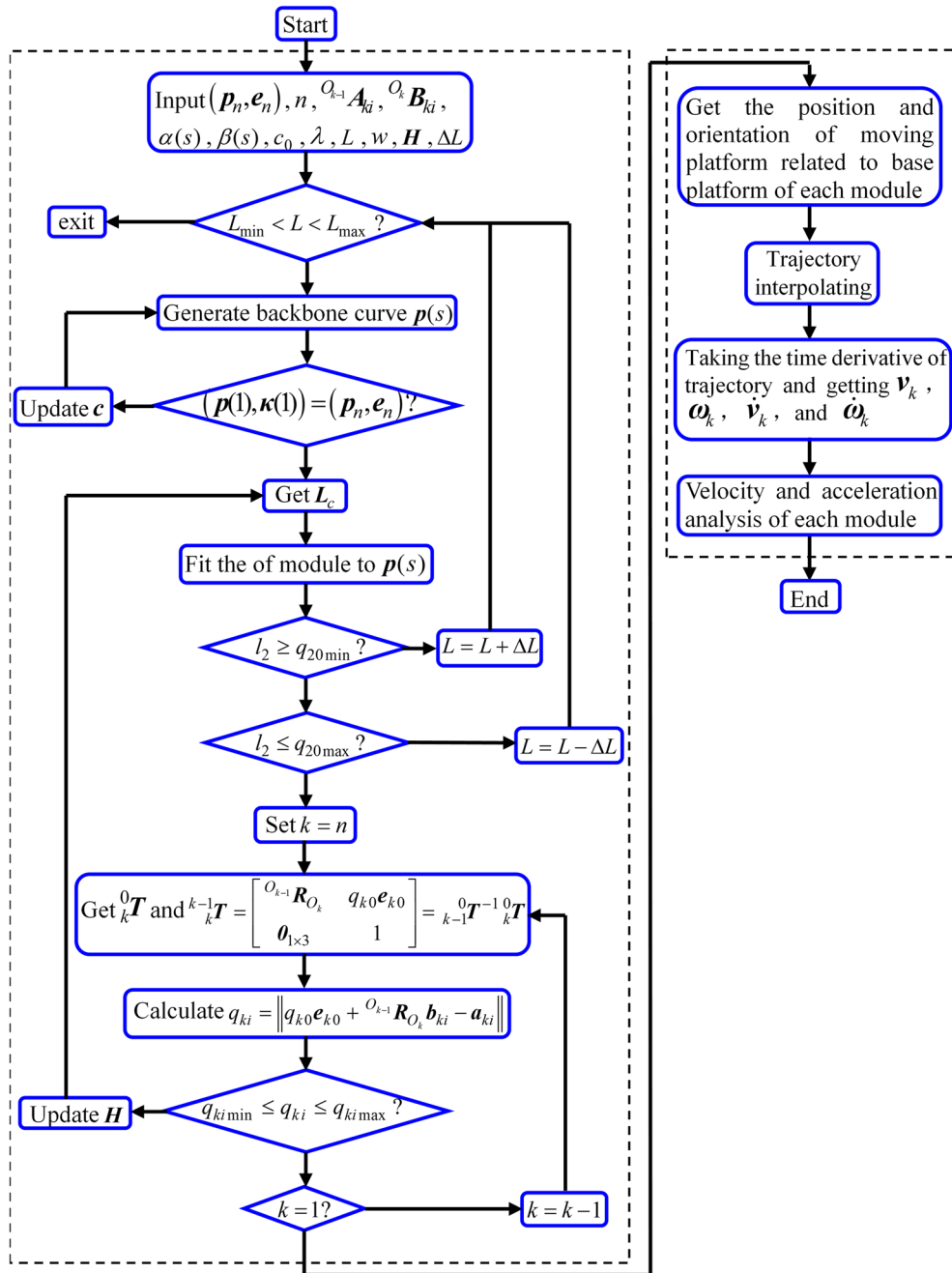


Figure 5 Kinematic algorithmic flow of the HRETR

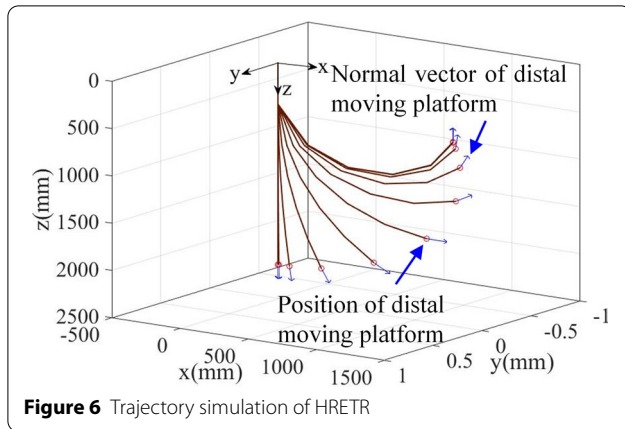


Figure 6 Trajectory simulation of HRETR

4.1 Dynamic Analysis of the HRETR

In order to ensure the reliability of the prototype, the dynamic analysis of the robot is carried out with virtual prototype technology before the prototype testing. On the basis of Section 3.1, MATLAB is used to carry out the kinematic simulation. The specific trajectory is shown in Eq. (15), and the trajectory data of each electric cylinder are obtained (Figure 6). The data are imported into the driving joint of the prototype (Figure 7). After the simulation, the displacement, velocity, acceleration and force curve of the driving joint of each unit parallel mechanism module can be obtained as outputs. The simulation results are shown in Figures 8, 9, 10, 11, 12, 13.

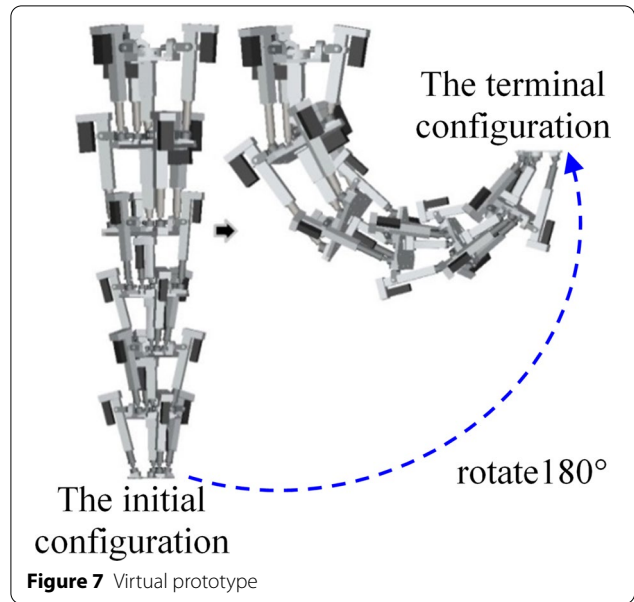


Figure 7 Virtual prototype

the dynamic diagram of Figures 8, 9, 10, 11, 12, 13, the range of the driving force of each limb in Module 1 and 2 is 0–3500 N, Module 3 is 0–2000 N, and Module 4, 5, and 6 is 0–1500 N. The electric cylinders of each module are selected based on Figures 8, 9, 10, 11, 12, 13. The rated driving force of the selected electric cylinders is shown in Table 1.

$$\left\{ \begin{array}{l} x = (432.6 + f_1(t)) \sin(f_2(t)) + (329.6 + f_1(t)) \sin(2f_2(t)) + \\ \quad (318 + f_1(t)) \sin(3f_2(t)) + (313 + f_1(t)) \sin(4f_2(t)) + (313 + \\ \quad f_1(t)) \sin(5f_2(t)), \\ y = 0, \\ z = (432.6 + f_1(t)) + (432.6 + f_1(t)) \cos(f_2(t)) + (329.6 + f_1(t)) \\ \quad \cos(2f_2(t)) + (318 + f_1(t)) \cos(3f_2(t)) + \\ \quad (313 + f_1(t)) \cos(4f_2(t)) + (313 + f_1(t)) \cos(5f_2(t)), \\ \phi_x = 0, \\ \phi_y = 8.48 \times 10^{-6} t^4 - 3.93 \times 10^{-7} t^5 + 4.71 \times 10^{-9} t^6 - 2.44 \times 10^{-11} t^7, \\ \phi_z = 0, \\ f_1(t) = 2.7 \times 10^{-5} t^4 - 1.08 \times 10^{-6} t^5 + 1.5 \times 10^{-8} t^6 - 7.14 \times 10^{-11} t^7, \\ f_2(t) = 1.41 \times 10^{-6} t^4 - 5.66 \times 10^{-8} t^5 + 7.86 \times 10^{-10} t^6 - 3.74 \times 10^{-12} t^7, \end{array} \right. \quad (15)$$

where x , y , z , ϕ_x , ϕ_y , and ϕ_z denote the position and orientation of the distal moving platform of the HRETR.

By observing the kinematic diagram of Figures 8, 9, 10, 11, 12, 13 the kinematic law of each limb meets the preset requirements (both the initial and terminal velocity and the acceleration are 0). By observing

4.2 Static Stiffness Analysis of the HRETR

In order to ensure that the designed components can meet the stiffness requirements, ANSYS is used to analyze the static stiffness of the HRETR. The results are shown in Figure 14.

The static stiffness of the HRETR is analyzed on some typical configurations by using software ANSYS. The

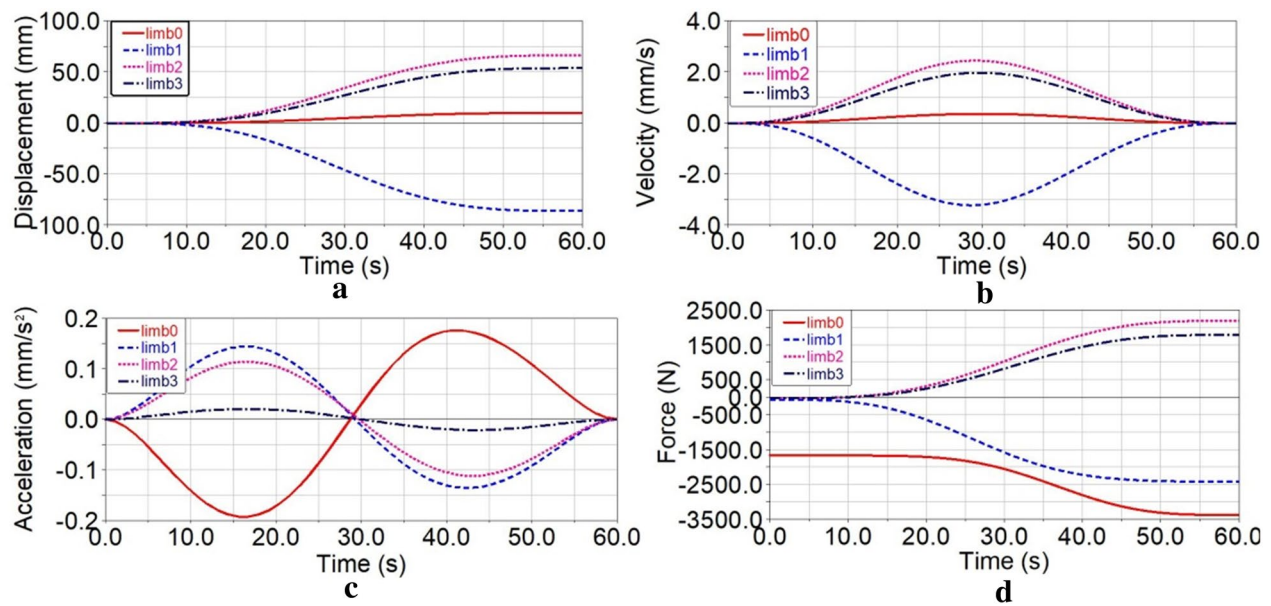


Figure 8 a Displacement, b velocity, c acceleration, and d driving force of each limb of module 1

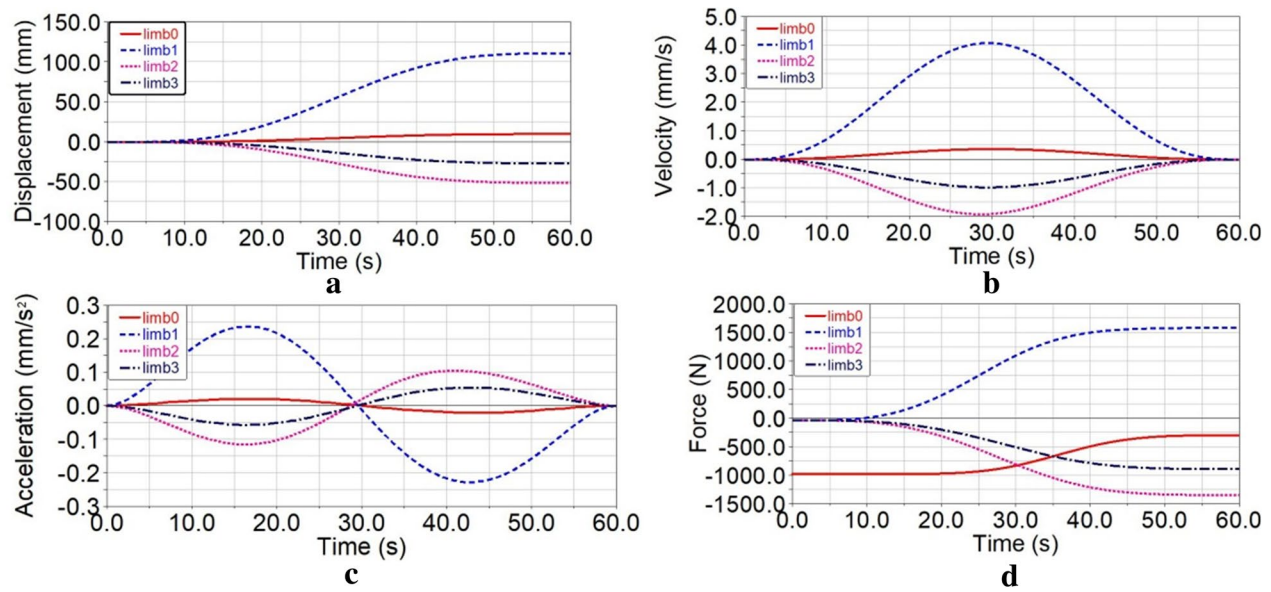


Figure 9 a Displacement, b velocity, c acceleration, and d driving force of each limb of module 2

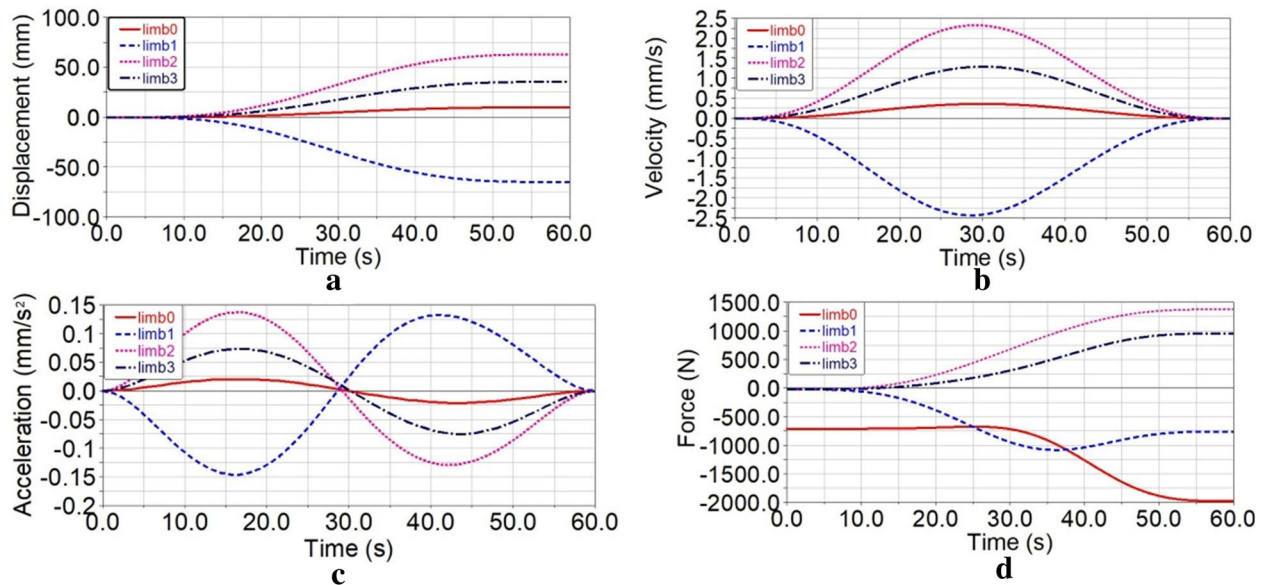


Figure 10 a Displacement, b velocity, c acceleration, and d driving force of each limb of module 3

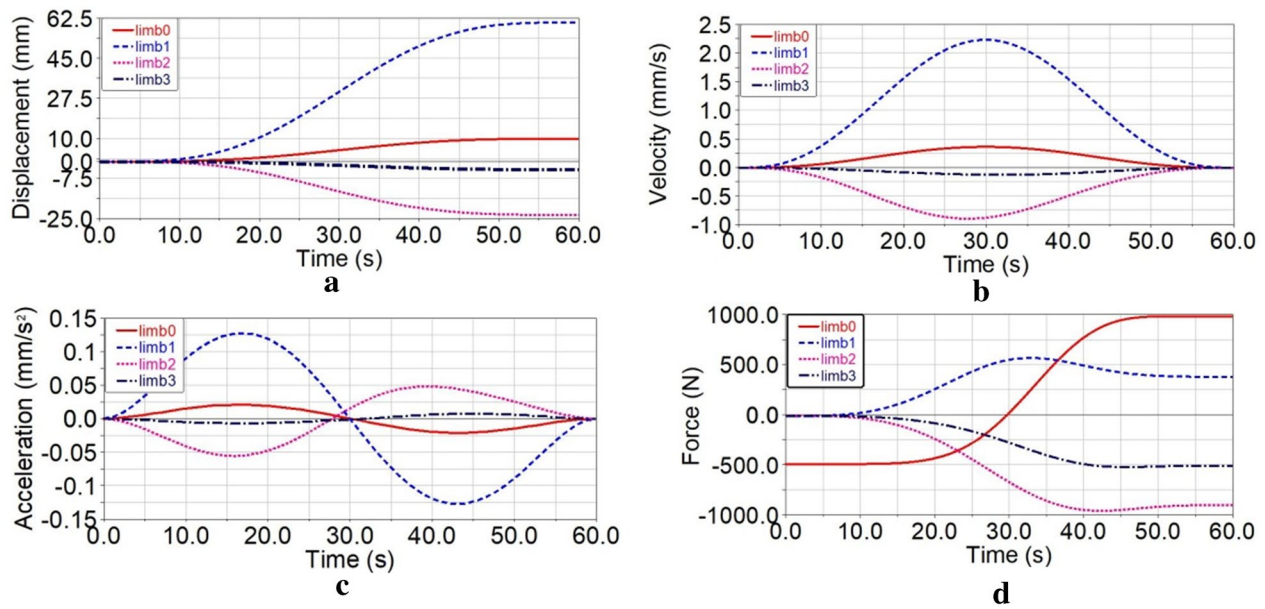


Figure 11 a Displacement, b velocity, c acceleration, and d driving force of each limb of module 4

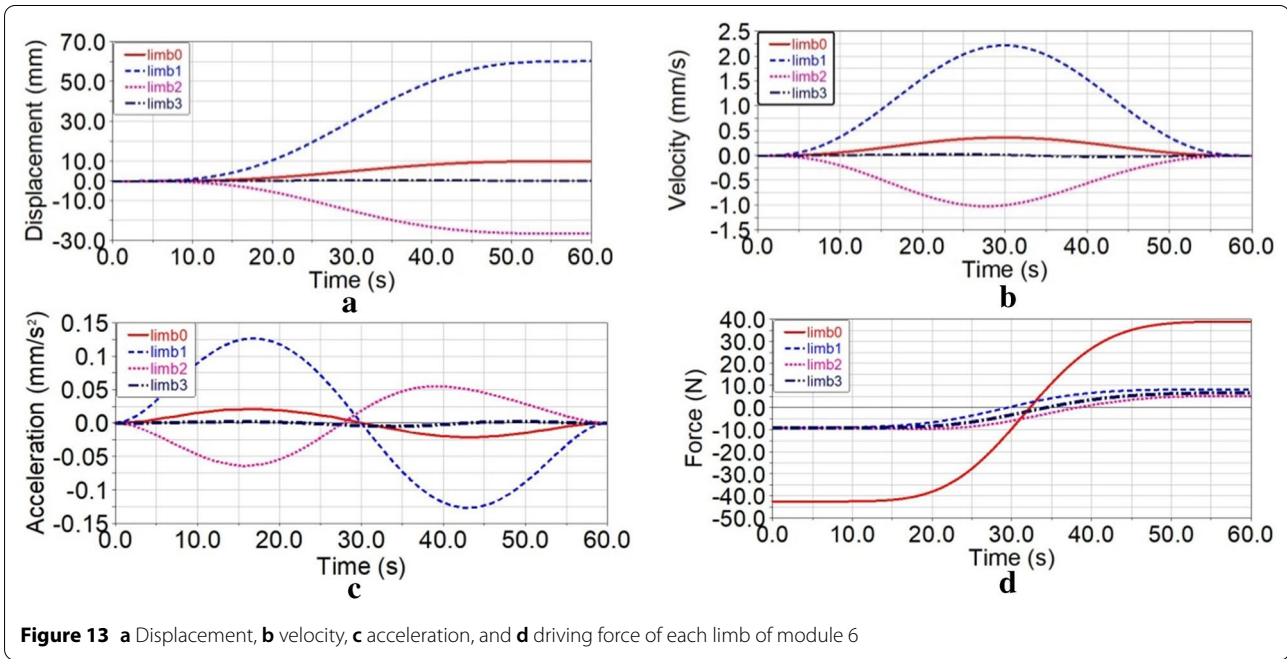
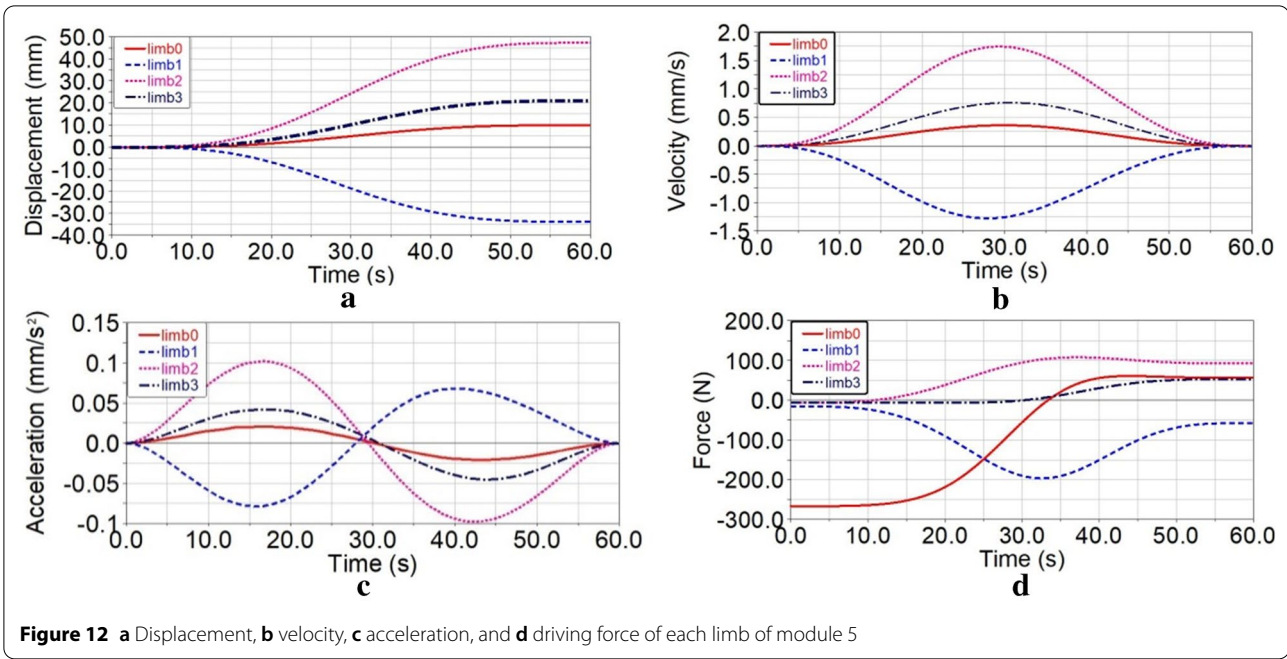
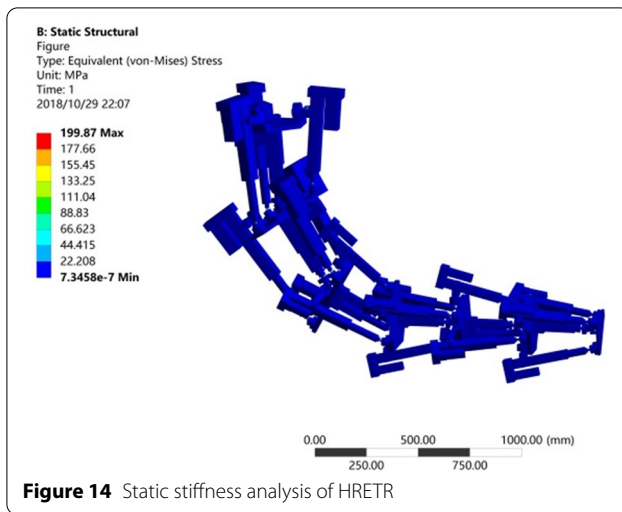


Table 1 Rated driving force of the electric cylinder in each module of the HRETR

| The <i>i</i> th module | <i>i</i> = 1 | <i>i</i> = 2 | <i>i</i> = 3 | <i>i</i> = 4 | <i>i</i> = 5 | <i>i</i> = 6 |
|-------------------------|--------------|--------------|--------------|--------------|--------------|--------------|
| Rated driving force (N) | 6000 | 6000 | 2500 | 2000 | 2000 | 2000 |

**Table 2** Properties of materials in key parts

| | Moving, base platform (7075 aluminum) | Key component (45#steel heat treatment) | Flange (cast iron) |
|------------------------|---------------------------------------|---|--------------------|
| Tensile strength (MPa) | 524 | 600 | 490 |
| Yield strength (MPa) | 455 | 355 | 330 |

maximum stress that is located on the external hinge of module 3 is 199.87 MPa. Compared with the material and mechanical properties of the key parts (Table 2), it meets the mechanical requirements.

5 Control System Design

The control system is divided into hardware design and software design. The design of the software and hardware follows the principle of hierarchical and modular design. Based on the established overall framework, the control system is divided into different modules according to its functions. This design principle facilitates subsequent maintenance and upgrading.

5.1 Software Design of the Control system

5.1.1 Integral Structure Design of Software of the Control System

The aim of the control system of the HRETR mainly aims to simulate a movement like an elephant's trunk. In the process of the motion, the control system needs to have a reliable kinematic calculation and trajectory planning interpolation algorithm, and it also needs to monitor the state of the real-time motion via a friendly control interface. At the same time, the design of the control system

software of the HRETR needs to consider the extensibility of structure of the robot in order to meet different working requirements. This software system adopts the modular design method. From the human-computer interaction interface to the hardware driver, the system is divided into four-fold: application layer, function layer, execution layer, and driver layer. The overall control architecture is shown in Figure 15.

5.1.2 Control Interface

The control interface is between the user and the robot control system. Most of the content of the robot is displayed on the control interface, thus providing the user with a concise and intuitive operation environment. Figure 16 shows the main interface of the control interface, which is composed of several modules. The main interface is used to display the current three-dimensional position and the orientation information of the robot, to query the current status of each mechanism parallel module, to record and display the user's operation and the running status of the system in real time, and to save the information in the log file. At the same time, it also includes the control system's function buttons, which control the motion planning, return home, parameter setting, starting, suspending, and exiting. The motion planning interface is shown in Figure 17. It can set up the motion planning parameters of the HRETR, including point motion, motion interpolation, and obstacle avoidance planning. The state monitoring and setting interface of the mechanism module is shown in Figure 18. It can monitor the status of each axis of the mechanism module, including the actual position, the planning position, the actual velocity, the planning velocity, and the planning acceleration.

5.2 Hardware Design of the Control System

The HRETR adopts the extensible hardware system platform of IPC + multi-motion control card. The hardware structure of the system is shown in Figure 19. In order to meet the interchangeability of the hardware system structure, the system hardware is divided into the industrial computer, the motion module, the servo drive module, the controller, the servo system module, and other main modules. These modules have relatively independent functions, and users can replace them based on their needs. The virtual prototype technology is used to simulate the motion of the prototype. The estimated parameters of important performance indexes such as rated torque and rated velocity of the servo motor are obtained in conjunction with the dynamic analysis in the virtual environment. The type of selected hardware of the control system is shown in Table 3.

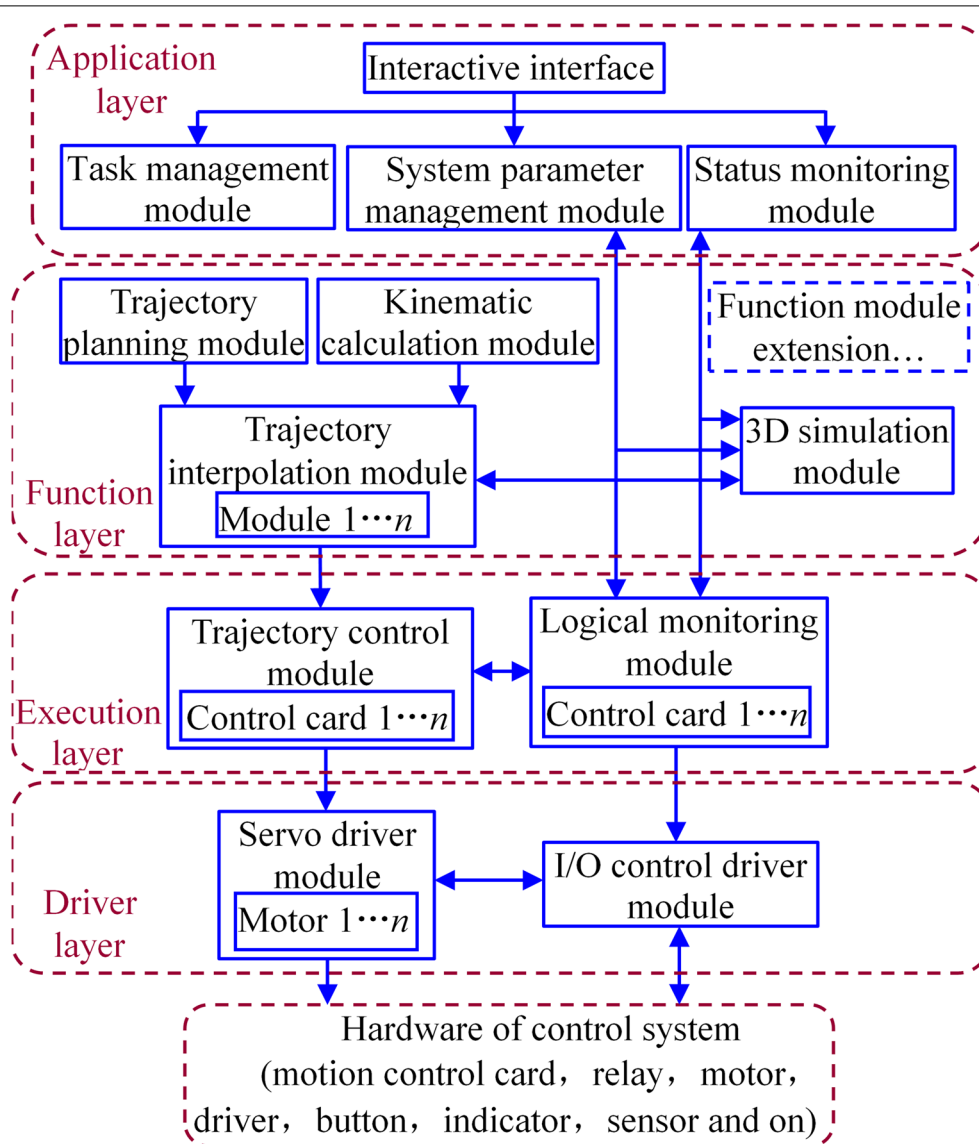


Figure 15 Software of the control system of the HRETR

6 Prototype Building

The prototype construction is the last stage in the development of the HRETR. It involves the problems of processing technology and engineering technology. In the construction process, the steps of installation, debugging, and operation need to be arranged properly and carried out orderly to minimize hazards and ensure personal safety. In order to improve the assembly efficiency, the

virtual prototype is simulated in SolidWorks to provide support for the assembly of the physical prototype. Also, the software must be installed efficiently and sequentially. The steps of building the physical prototype are shown in Figure 20.

It is necessary to test the performance of the prototype when the prototype is built. Before testing, it is necessary to import the control data obtained from the kinematic

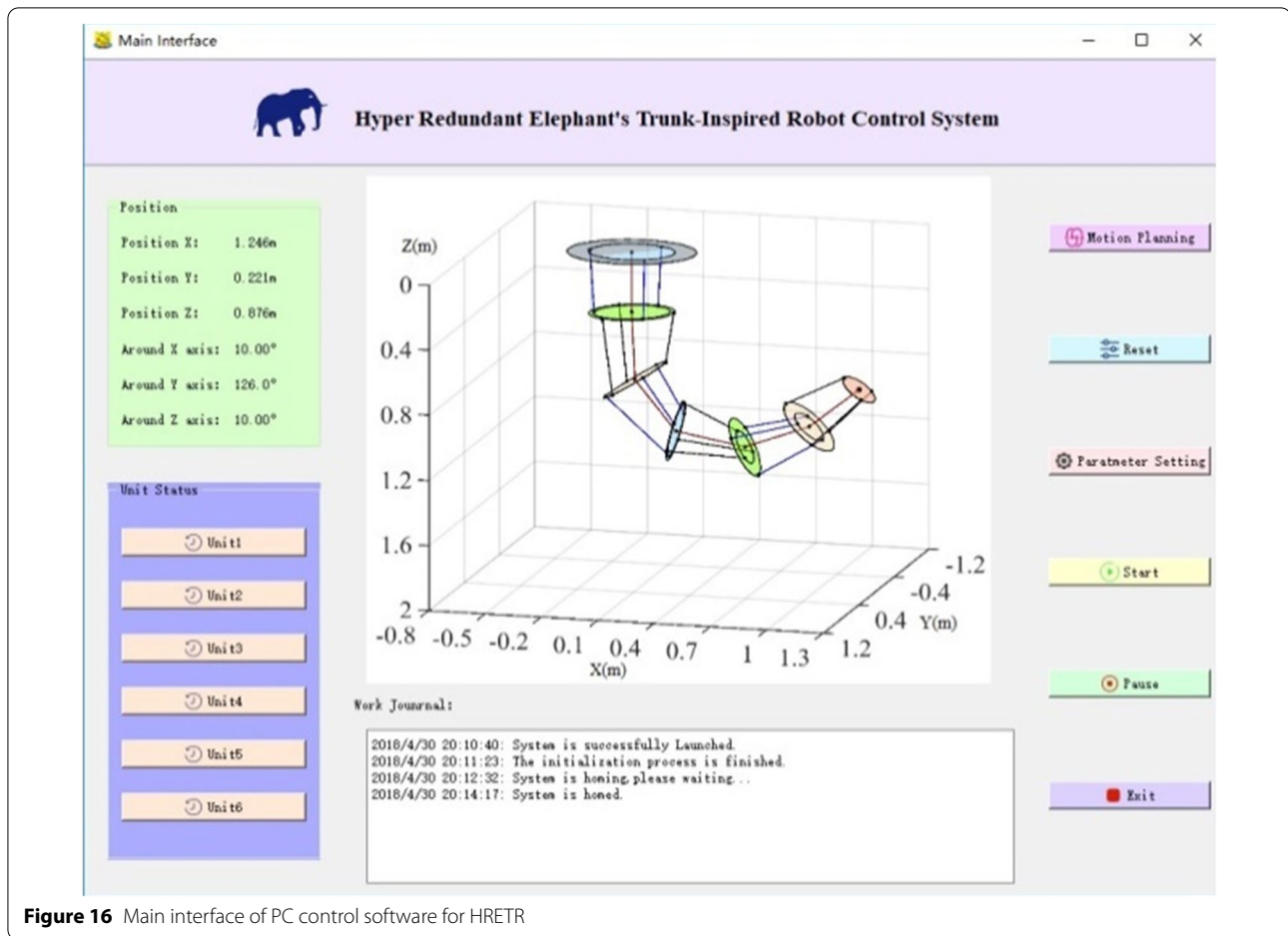


Figure 16 Main interface of PC control software for HRETR

model into the virtual prototype to observe whether there is a sudden change in the force of each limb in the motion process and whether the motion is stable. The testing process should be gradual. After the debugging process, the performance of each module is tested by letting the HRETR operate according to the given trajectory shown in Figures 21, 22, 23, 24, 25, 26. The results show that the robot can bend like an elephant's trunk in a wide range. Table 4 shows the motion performance of the HRETR.

7 Conclusions

In this paper, a prototype of a HRETR with expansibility is designed based on the principle of mechanical bionics while considering the special structure and movement mechanism of an elephant's trunk muscle group. A summary can be drawn as follows:

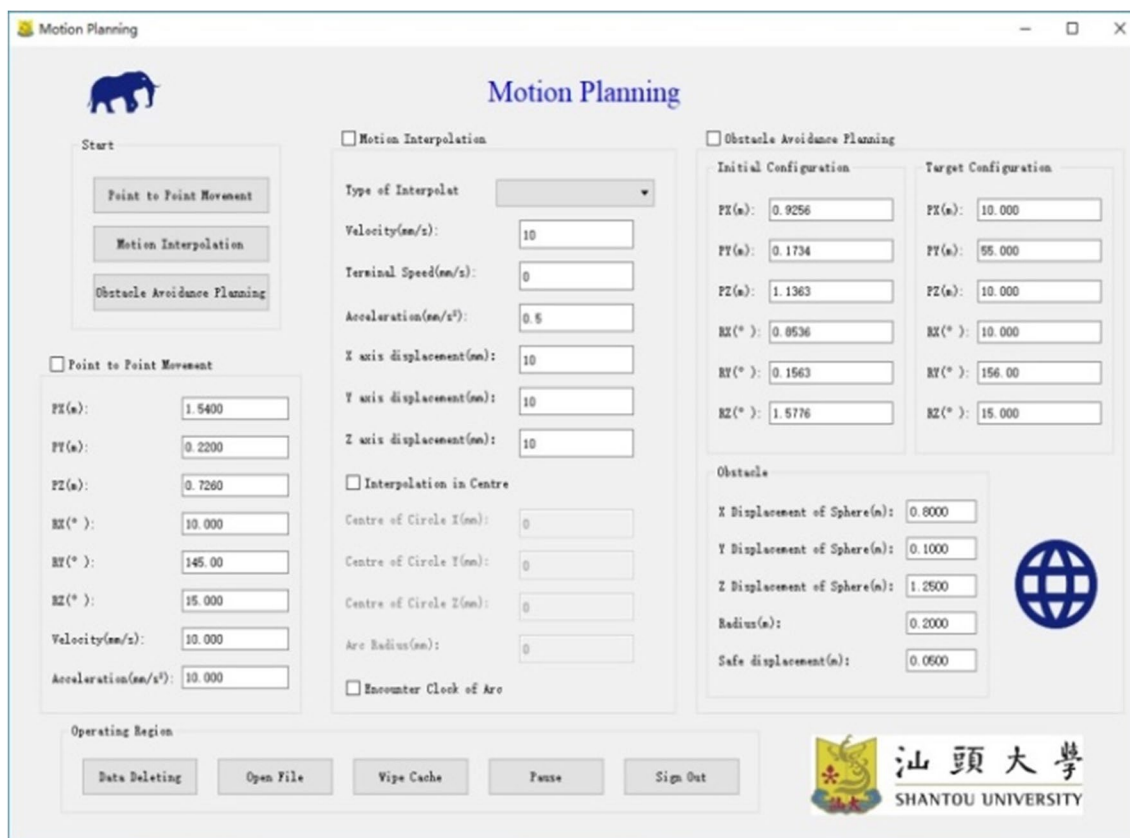


Figure 17 Interface of motion planning for HRETR

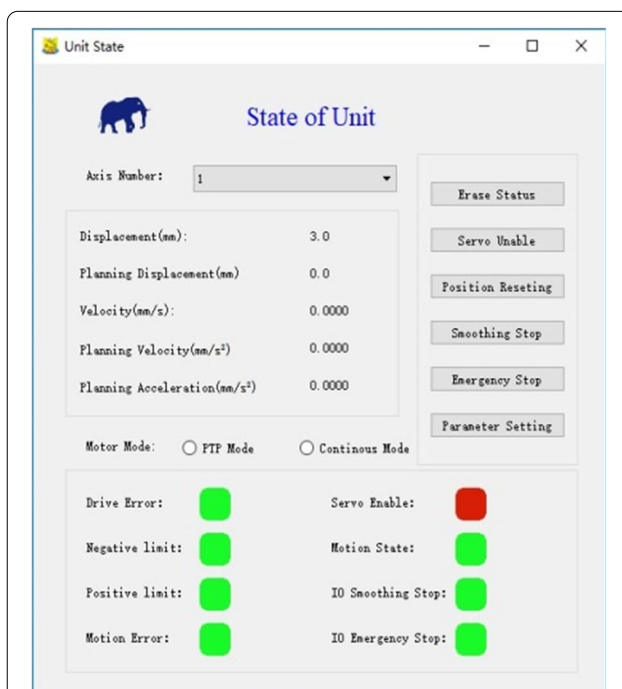


Figure 18 Status monitoring of parallel mechanism module

(1) Based on the principle of bionic design, a HRETR with an open structure which is composed of six modules of 3UPS-PS parallel mechanism in series is designed. Using the spatial backbone modal method, the kinematic model of this robot is established. The dynamic and the static stiffness of the robot are analyzed with virtual prototype technology, which provides the basis for the refinement of the structure, the selection of the prototype material and the electric cylinder.

(2) According to the structural characteristics of the HRETR, an extensible software and hardware control system is constructed according to the modular and hierarchical design criteria, a construction method that fully maximizes the potential extensibility of the HRETR.

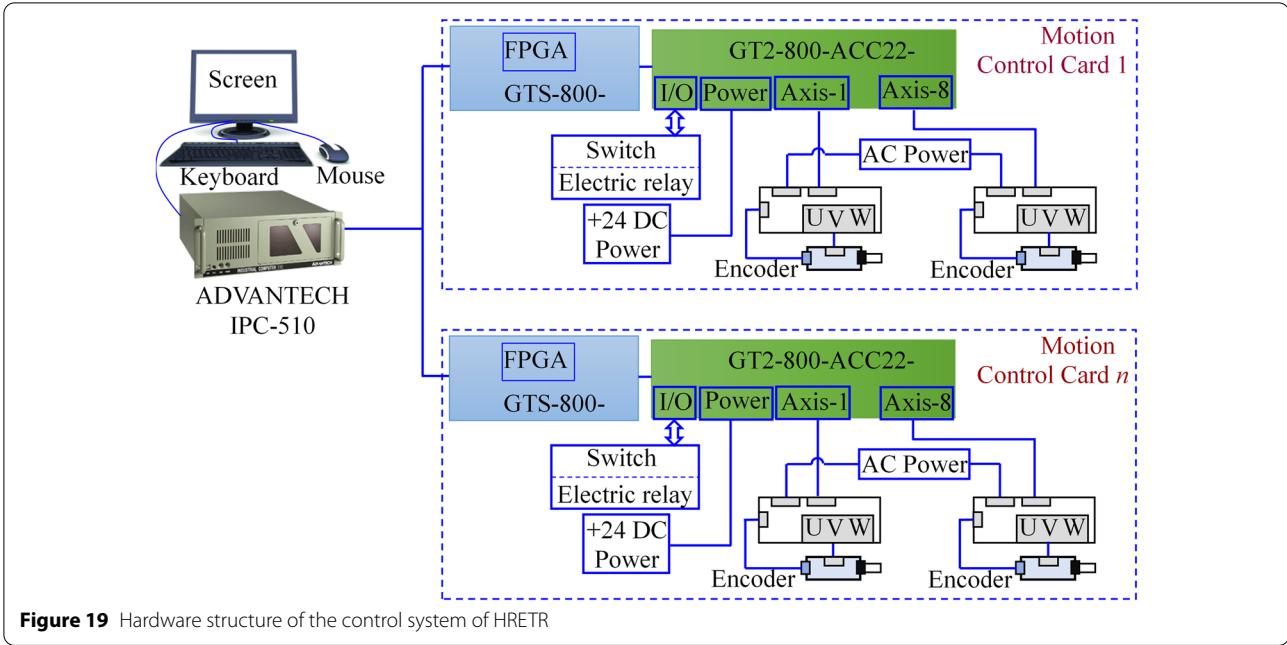


Figure 19 Hardware structure of the control system of HRETR

Table 3 Parameters of control system hardware

| Name | | | Parameter |
|---------------------|----------|--------------------|---|
| Industrial PC | | | Intel Core i7, 8G RAM |
| Motion control card | | | DSP processor, FPGA, PCI bus transmission, 8-axes servo control |
| Module 1, 2 | UPS limb | Servo motor driver | Power 400 W, rated speed 3000 r/min, rated torque 1.27 N m |
| | PS limb | Servo motor driver | Power 200 W, rated speed 3000 r/min, rated torque 0.64 N m |
| Module 3, 4, 5, 6 | UPS limb | Servo motor driver | Power 100 W, rated speed 3000 r/min, rated torque 0.32 N m |
| | PS limb | Servo motor | Power 100 W, rated speed 3000 r/min, rated torque 0.32 N m |

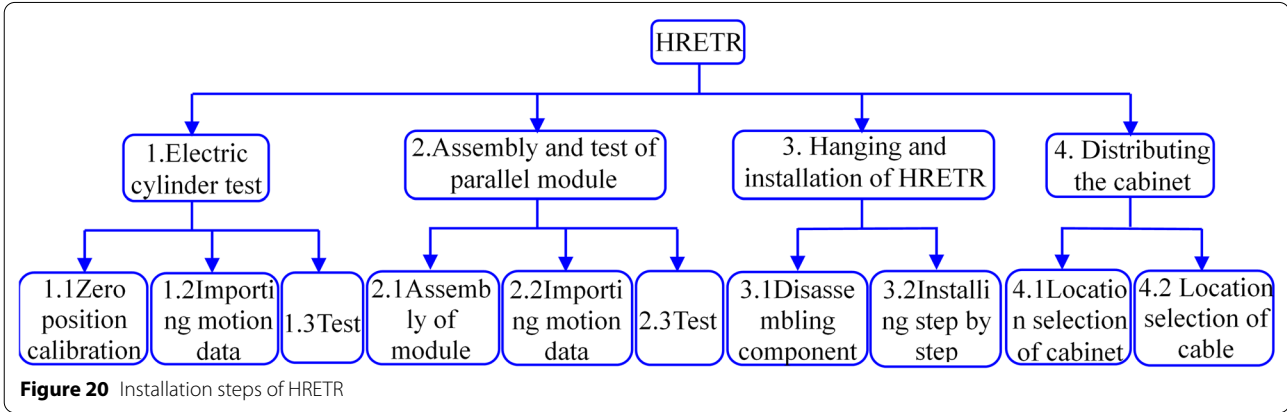


Figure 20 Installation steps of HRETR

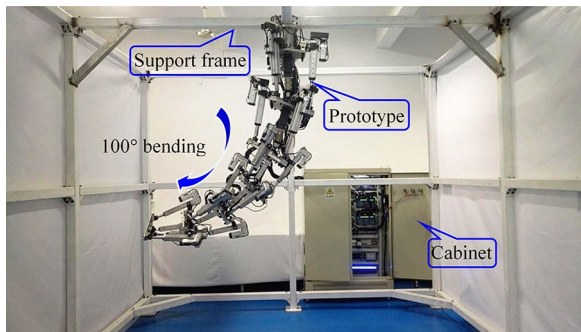


Figure 21 100° bending configuration of HRETR

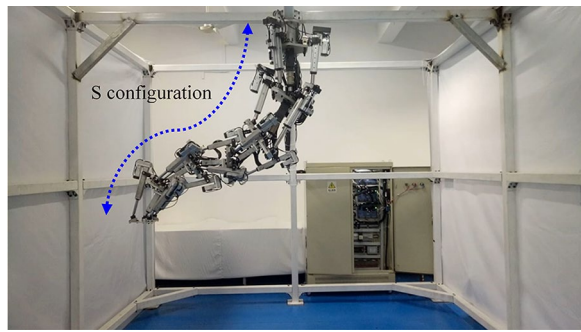


Figure 23 S configuration of HRETR

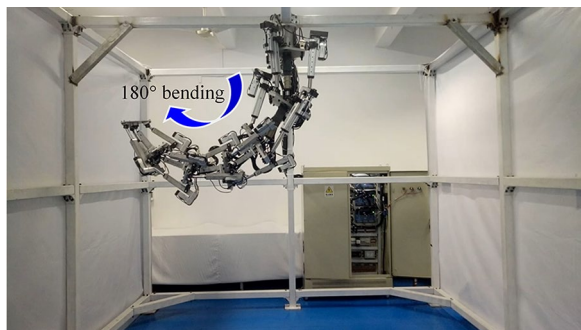


Figure 22 180° bending configuration of HRETR

(3) The performance of the prototype is tested and it is shown that the HRETR can realize the functions of bending like an elephant's trunk. This finding verifies the rationality and feasibility of the mechanical structure design and control method of the robot.

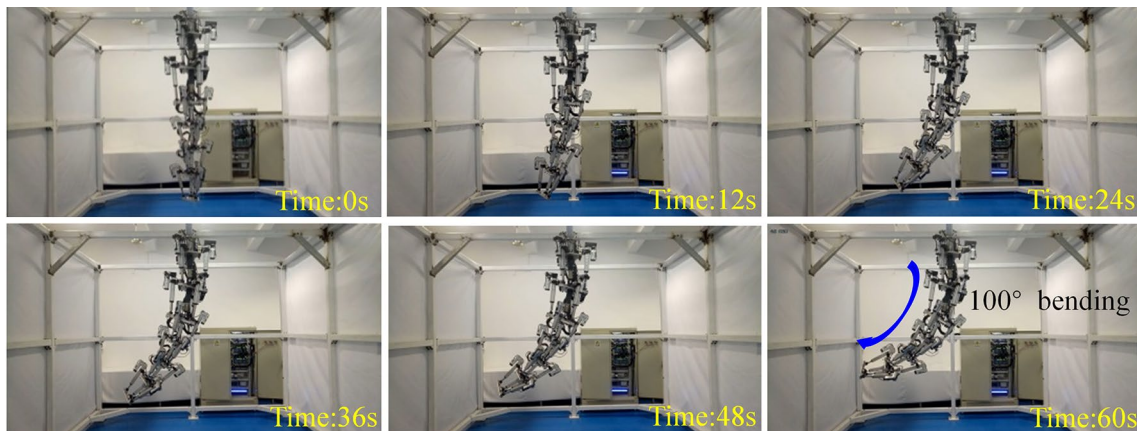


Figure 24 100° bending configuration of HRETR

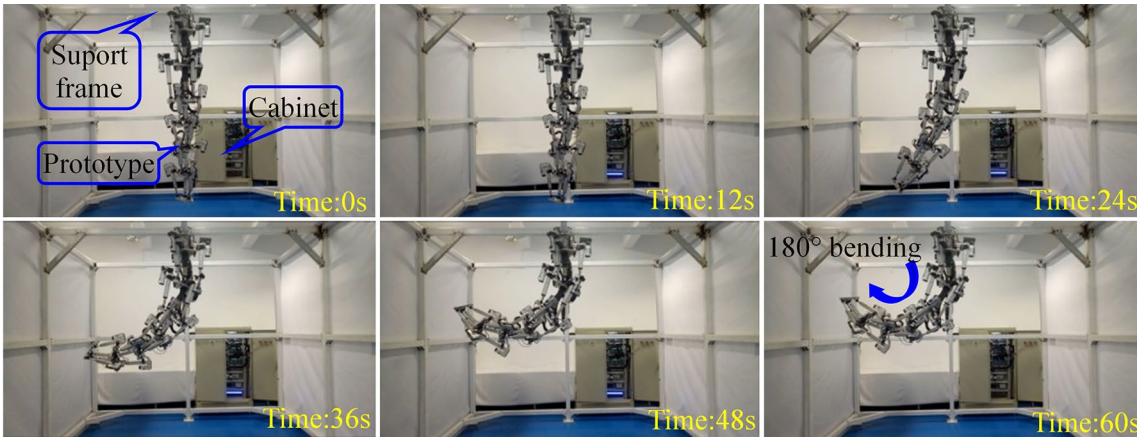


Figure 25 180° bending configuration of HRETR

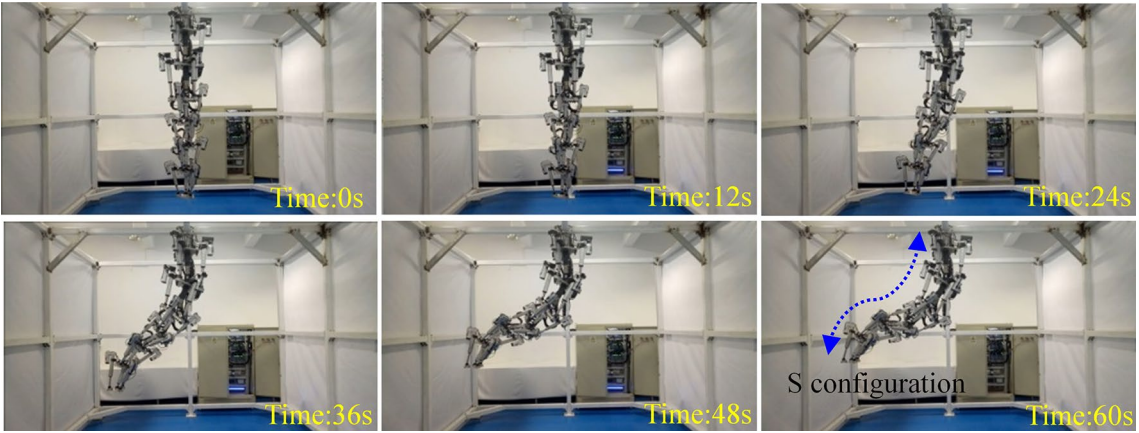


Figure 26 S configuration of HRETR

Table 4 Performance parameters of the HRETR

| Name | Module 1 | Module 2 | Module3 | Module4 | Module 5 | Module6 |
|---|---------------|----------|---------|---------|----------|---------|
| Angle of rotation along the x-axis | ± 30° | ± 30° | ± 30° | ± 30° | ± 30° | ± 30° |
| Angle of rotation along the y-axis | ± 30° | ± 30° | ± 30° | ± 30° | ± 30° | ± 30° |
| Angle of rotation along the z-axis | ± 60° | ± 60° | ± 60° | ± 60° | ± 60° | ± 60° |
| Angle of rotation along the x, y, z-axis simultaneously | ± 17° | ± 17° | ± 17° | ± 17° | ± 17° | ± 17° |
| Expansion range | ± 20mm | ± 20mm | ± 15mm | ± 25mm | ± 25mm | ± 25mm |
| Power of the module | 1400W | 1400W | 400W | 400W | 400W | 400W |
| Name | HRETR | | | | | |
| Angle of rotation along the x-axis | — 180°~180° | | | | | |
| Angle of rotation along the x-axis | — 180°~180° | | | | | |
| Angle of rotation along the x-axis | — 360°~360° | | | | | |
| Angle of rotation along the x, y, z-axis simultaneously | — 102°~102° | | | | | |
| Expansion range | — 130mm~130mm | | | | | |
| Power of the module | 4400W | | | | | |
| Maximum velocity of the electric cylinder | 25mm/s | | | | | |
| Response frequency of the system | 0Hz~20Hz | | | | | |
| Weight | 215kg | | | | | |
| Length | 2163mm~2423mm | | | | | |

Authors' contributions

YZ was in charge of the whole trial, wrote and revised the manuscript, also took part in the design, kinematics of the HRETR. XS took part in writing the manuscript, designing the control system, and building prototype. XZ took part in the simulation. XL took part in the building prototype. All authors read and approved the final manuscript.

Authors' information

Yongjie Zhao, born in 1977, is currently a Professor at *Shantou University, Shantou, China*. He received the B.E. degree in metallurgy engineering from *Northeast University, China*, in 2000, the M.E. degree in mechanical engineering from *Tianjin University of Technology, Tianjin, China*, in 2003, and the Ph.D. degree in mechanical engineering from *Tianjin University, Tianjin, China*, in 2006. From 2006 to 2008, he worked as a postdoctoral research fellow at *State Key Laboratory of Mechanical System and Vibration, Shanghai Jiao Tong University, Shanghai, China*. His current research interests include kinematics, dynamics, performance evaluation and control, multidisciplinary optimization design of manipulators.

Xiaogang Song, born in 1993, is currently a PhD candidate at *Harbin Institute of Technology, Shenzhen, China*. He received the B.E. degree in mechanical design, manufacturing and automation from *Qingdao University of Technology, Qingdao College, Qingdao, China*, in 2016, and the M.E. degree in mechanical engineering from *Shantou University, Shantou, China*, in 2019. His current research interests include kinematics, dynamics, and control of manipulators.

Xingwei Zhang, born in 1980, is currently an Associate Professor at *Department of Mechatronics Engineering, Shantou University, China*. He obtained the B.E. degree in thermal energy and power engineering in 2003, the M.E. degree in mechanical and electronic engineering in 2006 and the Ph.D. degree in fluid machinery and engineering in 2011, all from *Harbin Institute of Technology, China*. He is mainly engaged in the design of special bionic robots, design and analysis of bionic mechanical structures, fluid force reduction and flow control research direction.

Xinjian Lu, born in 1962, is the General Manager of *Guangdong Goldenwork Robot Technology Ltd, Foshan, China*. He received the B.E. degree in aerospace welding engineering from *Nanchang Hangkong University, China*, in 1983. His current research interests include robot application and welding robot.

Funding

Supported by National Natural Science Foundation of China (Grant No. 51375288), Science and Technology Program of Guangdong Province of China (Grant No. 2020ST004), Department of Education of Guangdong Province of China (Grant No. 2017KZDXM036), and Special Project for Science and Technology Innovation Team of Foshan City of China (Grant No. 2018IT100052).

Competing interests

The authors declare no competing financial interests.

Author Details

¹ Department of Mechatronics Engineering, Shantou University, Shantou 515063, China. ² Guangdong Goldenwork Robot Technology Ltd., Foshan 528226, China.

Received: 13 October 2019 Revised: 2 November 2020 Accepted: 11 November 2020

Published online: 09 December 2020

References

- [1] P J Alhama Blanco, F J Abu-Dakka, M Abderrahim. Practical use of robot manipulators as intelligent manufacturing systems. *Sensors*, 2018, 18(9): 1–12.
- [2] S M Wang, K F Ehmann. Error model and accuracy analysis of a six-dof Stewart platform. *Journal of Manufacturing Science and Engineering*. 2016, 124(2): 286–295.
- [3] C Connolly. ABB high-speed picking robots establish themselves in food packaging. *Industrial Robot*, 2007, 34(4): 281–284.
- [4] J C Shin, C W Lee. Rider's net moment estimation using control force of motion system for bicycle simulator. *Journal of Robotic System*, 2004, 21(11): 597–607.
- [5] L Fang, F Gao. Type design and behavior control for six legged robots. *Chinese Journal of Mechanical Engineering*, 2018, 31: 59. <https://doi.org/10.1186/s10033-018-0259-9>.
- [6] Y G Li, Q S Xu. Design and development of a medical parallel robot for cardiopulmonary resuscitation. *IEEE/ASME Transactions on Mechatronics*, 2007, 12(3): 265–273.
- [7] J Burgner-Kahrs, D C Rucker, H Choset. Continuum robots for medical applications: a survey. *IEEE Transactions on Robotics*, 2015, 31(6): 1261–1280.
- [8] W He, S S Ge, Y A Li, E Chew, et al. Neural network control of a rehabilitation robot by state and output feedback. *Journal of Intelligent & Robotic Systems*, 2015, 80(1): 15–31.
- [9] G K Zhang, X Y Ren, J H Li, K Kong, et al. Modified pre-stretching assembly method for cable-driven systems. *Chinese Journal of Mechanical Engineering*, 2019, 32: 48. <https://doi.org/10.1186/s10033-019-0362-6>.
- [10] D S Zhang, Y D Xu, J T Yao, et al. Analysis and optimization of a spatial parallel mechanism for a new 5-DOF hybrid serial-parallel manipulator. *Chinese Journal of Mechanical Engineering*, 2018, 31: 54.
- [11] G Gibbs, S Sachdev. Canada and the international space station program: overview and status. *Acta Astronaut*, 2002, 51(1-9): 591–600.
- [12] A Flores-Abad, O Ma, K Pham, et al. A review of space robotics technologies for on-orbit servicing. *Progress in Aerospace Sciences*, 2014, 68(8): 1–26.
- [13] B Sangiovanni, G P Incremona, M Piastra, et al. Self-configuring robot path planning with obstacle avoidance via deep reinforcement learning. *IEEE Control Systems Letters*, 2021, 5(2): 397–402.
- [14] Y J Zhao, L Jin, P Zhang, et al. Inverse displacement analysis of a hyper-redundant elephant's trunk robot. *Journal of Bionic Engineering*, 2018, 15(2): 397–407.
- [15] Y-J Kim, S B Cheng, S Kim, et al. A stiffness-adjustable hyperredundant manipulator using a variable neutral-line mechanism for minimally invasive surgery. *IEEE Transactions on Robotics*, 2014, 30(2): 382–395.
- [16] G S Chirikjian, J W Burdick. The kinematics of hyper-redundant robot locomotion. *IEEE Transactions on Robotics and Automation*, 1995, 11(6): 781–793.
- [17] Y M Li, P S Ma, C J Qin, et al. Design and study of a novel hyper-redundant manipulator. *Robotica*, 2003, 21(5): 505–509.
- [18] B Hu, Y Wang, J J Yu, et al. Solving kinematics and stiffness of a novel n(2-UPS/PS+RPS) spatial hyper-redundant manipulator. *Robotica*, 2016, 34(10): 2386–2399.
- [19] J Gallardo-Alvarado, C R Aguilar-Nájera, L Casique-Rosa, et al. Solving the kinematics and dynamics of a modular spatial hyper-redundant manipulator by means of screw theory. *Multibody System Dynamics*, 2008, 20(4): 307–325.
- [20] H Yuan, Z Li. Workspace analysis of cable-driven continuum manipulators based on static mode. *Robotics and Computer-Integrated Manufacturing*, 2018, 49: 240–252.
- [21] B A Jones, W McMahan, I Walker. Design and analysis of a novel pneumatic manipulator. *Proceeding of 3rd IFAC Symposium on Mechatronic Systems*, 2004, 37(14): 687–692.
- [22] H S Wang, W D Chen, X J Yu, et al. Visual servo control of cable-driven soft robotic manipulator. *IEEE/RSJ International Conference on Intelligent Robots and Systems (ICIRS) IEEE*, 2013, 8125(2): 57–62.
- [23] A Chibani, C Mahfoudi, T Chettibi, et al. Generating optimal reference kinematic configurations for hyper-redundant parallel robots. *Institution of Mechanical Engineers*, 2015, 229(9): 867–882.
- [24] A A Transteth, R Leine, C Glocker, et al. 3-D snake robot motion: non-smooth modeling, simulations, and experiments. *IEEE Transactions on Robotics*, 2008, 24(2): 361–376.
- [25] A A Transteth, R I Leine, C Glocker, et al. Snake robot obstacle-aided locomotion: modeling, simulations, and experiments. *IEEE Transactions on Robotics*, 2008, 24(1): 88–104.
- [26] J Gallardo, H Orozco, J M Rico, et al. A new spatial hyper-redundant manipulator. *Robotics and Computer-Integrated Manufacturing*, 2009, 25(4): 703–708.
- [27] A Taherifar, H Salarieh, A Alasty. Kinematic control of a new hyper-redundant manipulator with lockable joints. *Scientia Iranica*, 2013, 20(6): 1742–1752.

- [28] Y J Zhao, Z Q Zhang, G Cheng. Inverse rigid-body dynamic analysis for a 3UPS-PRU parallel robot. *Advances in Mechanical Engineering*, 2017, 9(2): 1–14.
- [29] Y J Zhao, G Cheng. Dimensional synthesis of a 3UPS-PRU parallel robot. *Robotica*, 2017, 35(12): 2319–2329.
- [30] Y J Zhao. Dynamic optimum design of a 3UPS-PRU parallel robot. *Journal of Advanced Robotic System*, 2016, 13(6): 1–13.

Submit your manuscript to a SpringerOpen[®] journal and benefit from:

- Convenient online submission
- Rigorous peer review
- Open access: articles freely available online
- High visibility within the field
- Retaining the copyright to your article

Submit your next manuscript at ► [springeropen.com](https://www.springeropen.com)
